



**HAL**  
open science

# Numerical analysis of two-phase flow in condensers and evaporators with special emphasis on single-phase - two-phase transition zones

S. Morales-Ruiz, J. Rigola, C.D. Pérez-Segarra, O. García-Valladares

## ► To cite this version:

S. Morales-Ruiz, J. Rigola, C.D. Pérez-Segarra, O. García-Valladares. Numerical analysis of two-phase flow in condensers and evaporators with special emphasis on single-phase - two-phase transition zones. Applied Thermal Engineering, 2010, 29 (5-6), pp.1032. 10.1016/j.applthermaleng.2008.05.017 . hal-00619274

**HAL Id: hal-00619274**

**<https://hal.science/hal-00619274>**

Submitted on 6 Sep 2011

**HAL** is a multi-disciplinary open access archive for the deposit and dissemination of scientific research documents, whether they are published or not. The documents may come from teaching and research institutions in France or abroad, or from public or private research centers.

L'archive ouverte pluridisciplinaire **HAL**, est destinée au dépôt et à la diffusion de documents scientifiques de niveau recherche, publiés ou non, émanant des établissements d'enseignement et de recherche français ou étrangers, des laboratoires publics ou privés.

## Accepted Manuscript

Numerical analysis of two-phase flow in condensers and evaporators with special emphasis on single-phase - two-phase transition zones

S. Morales-Ruiz, J. Rigola, C.D. Pérez-Segarra, O. García-Valladares

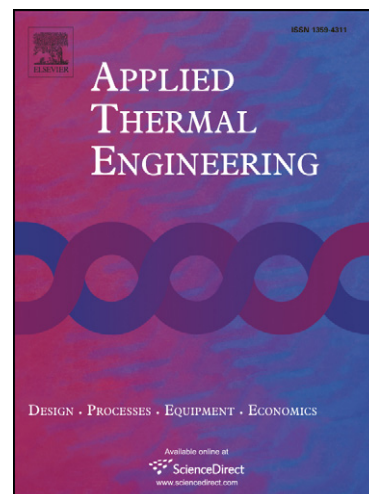
PII: S1359-4311(08)00234-2  
DOI: [10.1016/j.applthermaleng.2008.05.017](https://doi.org/10.1016/j.applthermaleng.2008.05.017)  
Reference: ATE 2520

To appear in: *Applied Thermal Engineering*

Received Date: 1 October 2007  
Revised Date: 2 April 2008  
Accepted Date: 19 May 2008

Please cite this article as: S. Morales-Ruiz, J. Rigola, C.D. Pérez-Segarra, O. García-Valladares, Numerical analysis of two-phase flow in condensers and evaporators with special emphasis on single-phase - two-phase transition zones, *Applied Thermal Engineering* (2008), doi: [10.1016/j.applthermaleng.2008.05.017](https://doi.org/10.1016/j.applthermaleng.2008.05.017)

This is a PDF file of an unedited manuscript that has been accepted for publication. As a service to our customers we are providing this early version of the manuscript. The manuscript will undergo copyediting, typesetting, and review of the resulting proof before it is published in its final form. Please note that during the production process errors may be discovered which could affect the content, and all legal disclaimers that apply to the journal pertain.



# Numerical analysis of two-phase flow in condensers and evaporators with special emphasis on single-phase - two-phase transition zones.

S. Morales-Ruiz <sup>a</sup>, J. Rigola <sup>a</sup>, C.D. Pérez-Segarra <sup>a,\*</sup>,  
O. García-Valladares <sup>b</sup>

<sup>a</sup>*Centre Tecnològic de Transferència de Calor (CTTC); Universitat Politècnica de Catalunya (UPC); ETSEIAT, Colom 11, 08222 Terrassa (Barcelona), Spain.*

<sup>b</sup>*Centro de Investigación en Energía (CIE), Universidad Nacional Autónoma de México (UNAM) Privada Xochicalco S/N, Temixco, 62580, Morelos, México*

---

## Abstract

A numerical study of the thermal and fluid-dynamic behaviour of the two-phase flow in ducts under condensation or evaporation phenomena is presented. The numerical simulation has been developed by means of the finite volume technique based on a one-dimensional and transient integration of the conservative equations (continuity, momentum and energy). The discretized governing equations are solved using the Semi-Implicit Method for Pressure-Linked Equations (SIMPLE) which allows back flow phenomena. Special emphasis is performed on the treatment of the transition zones between the single-phase and two-phase flow. The empirical inputs of single-phase and two-phase flow, including sub-cooled boiling and dry-out, have been adapted by means of adequate splines in the transition zones where the heat transfer correlations available in the literature are not suitable. Different numerical aspects have been evaluated with the aim of verifying the quality of the numerical

solution. The mathematical model has been validated by comparison with experimental data obtained from literature considering condensation and evaporation processes. This comparison shown the improvements in the numerical solution not only in the transition zone but also in all condenser and evaporator ducts, when the special treatment for transitions is used. Illustrative results on double-pipe heat exchanger are also presented.

*Key words:* Numerical simulation, two-phase flow, condensers, evaporators, transition zones, double-pipe heat exchangers.

---

## 1 INTRODUCTION

Heat exchangers are widely used in industrial applications, e.g. refrigeration and air-conditioning systems, where these equipments represent an important component. Condensers and evaporators in a vapour compression refrigeration system are an example. These elements have been studied for many years, and different experimental and mathematical modelling have been trying to explain the thermal and fluid dynamic behaviour of the fluid flow into the heat exchanger.

In many condensers and evaporators the fluid refrigerant flows inside tubes while the secondary fluid flows in the external part. In the refrigeration system, the heat exchanger are connected to other elements like compressors, expansion devices, receivers, etc. which have influence on the heat exchanger behaviour. The necessity of building equipment with higher energy efficiency and using non-contaminant refrigerants are important reasons for the continuous study and research on this topic.

---

\* Corresponding author. Tel. +34-93-739-81-92; fax: +34-93-739-81-01

*Email addresses:* [cttc@cttc.upc.edu](mailto:cttc@cttc.upc.edu), <http://www.cttc.upc.edu>, (C.D. Pérez-Segarra ).

The design of the heat exchanger can be developed by means of analytical methods. These methods give a quick and global approach of their behaviour. However, a large number of hypothesis and simplifications have to be assumed. Examples are the  $F - factor$  or  $\epsilon - NTU$  methods [1]. More general and accurate approaches require the use of numerical methodologies, which subdivide the heat exchanger into many elemental volumes and solve the governing equations for each volume. In the two-phase flow region, the governing equations (mass, momentum and energy) can be formulated in different forms depending on the model used. Homogeneous models [2], drift-flux models [3] or two-fluid models [4][5] can be employed to solve the two-phase flow present in the condensation and evaporation process.

To get a deep understanding of the mathematical model and the strategies for solving the governing equations, the double-pipe heat exchanger can be a good option for application due to its relatively simple geometry for the secondary flow. Different papers have been presented in the technical literature on this subject. For example, numerical and analytical results in steady and transient state have been compared in different studies on double-pipe heat exchangers [6][7][8]. Combination of the analytical expressions with numerical method are used in the double-pipe helical heat exchanger resolution [9], where a CFD modelling together with a  $\epsilon - NTU$  method is used to solve the heat exchanger. Assuming thermodynamic non-equilibrium on the CV, the two-fluid model is used to solve the two-phase flow inside of the double-pipe heat exchanger. A condenser and evaporator are solved by means of this model in [10] and [11], respectively. Although this formulation shows the two-phase flow behaviour in a more detailed way, a large number of the empirical information is required and different hypothesis have to be assumed to simplify the resolution. A quasi-homogeneous model is used on double-pipe heat exchangers resolution [12] and [13], where one-dimensional single-phase and two-phase flow are solved based on an implicit step by step method.

This paper shows a more general approach for the resolution of the two-phase flow inside tubes in condensers and evaporators. The methodology is applied to double-pipe heat exchangers with the secondary fluid in the annulus region. This work is organised in different sections. The second section shows the mathematical formulation of the whole heat exchanger. Special attention is given to the analysis of the two-phase flow inside tubes by means of the Semi-Implicit Method for Pressure-Linked Equations (SIMPLE) [14] instead of the step-by-step method employed by the authors [12] and [13]. The SIMPLE method is able to solve complex flow phenomena, e.g. when back flow appears due the interactions of the heat exchangers with other elements of the refrigeration system (compressor, expansion device, receivers, etc.). The third section presents the numerical algorithm, together with different important aspects used in the solution. New criteria for the analysis of the transition zones to avoid discontinuities in the evaluation of the heat transfer coefficients between single-phase and two-phase are presented. This is an important topic that helps to prevent the appearance of non real wall temperature values and improves the numerical method. The fourth section shows the methodology to verify the numerical solutions to assure the quality of the results obtained. The mathematical model is validate in the fifth section by comparisons of the well verified numerical results with experimental data obtained from the scientific literature. Illustrative results considering the whole double-pipe heat exchanger are given in section sixth. In the last section, the conclusions of the paper are presented.

## **2 MATHEMATICAL FORMULATION AND DISCRETIZED EQUATIONS**

This section presents the mathematical formulation for the whole double-pipe heat exchanger, i.e. the two-phase flow of refrigerant in the inner tube (sub-

sections 2.1), the secondary fluid in the annulus (subsections 2.2), and the solids elements: inner tube, outer tube and insulator (subsection 2.3). A final subsection shows the empirical inputs needed to take into account fluid-solid interactions.

The main assumed hypothesis in the fluid flows are: one-dimensional flow, quasi-homogeneous model, negligible axial heat conduction and viscous stress in fluid and negligible heat radiation. The assumed hypothesis in the solid elements are: one-dimensional transient temperature distribution along inner and outer tubes length (but two-dimensional heat flux distribution), two-dimensional transient axisymmetric temperature and heat flux distribution in the insulator, and negligible heat radiation between tubes in the annulus and between insulator and the exterior.

The mathematical formulation is based on the conservation equations of mass, linear momentum and energy for the fluids and the energy equation for the solid elements.

For the fluids, these equations are integrated on the basis of staggered meshes. In this way, the domain is split into a number of control volumes (CVs). Mass and energy equations are discretized over the main CVs (see Figure 1a), while momentum equation is discretized over the staggered CVs as shown in Figure 1b. For the solid elements, the energy equation is discretized over CVs indicated in Figure 2.

### *2.1 Two-phase flow of refrigerant Fluid*

The discretized form of the energy, momentum and mass (in terms of the pressure corrections) conservations equation of the refrigerant flow inside the inner tube is presented in this subsections.

*Energy equation*

The total energy equation is integrated over the main control volumes shown in Figure 1a. In a semi-discretized form, this equation can be written as:

$$\frac{\partial \tilde{\rho}_P \bar{e}_P}{\partial t} A \Delta z + \dot{m}_P^s e_e - \dot{m}_W^s e_w = \bar{q}_P P \Delta z + \frac{\partial \tilde{p}_P}{\partial t} A \Delta z \quad (1)$$

where  $\bar{e}_P$  represents the total specific energy ( $e = h + e_c + e_p$ ),  $\tilde{\rho}_P$  is the density,  $\bar{q}_P$  is the heat flux,  $\tilde{p}_P$  is the pressure,  $\dot{m}_P^s$  and  $\dot{m}_W^s$  are the mass flow at the east and west CV-faces respectively,  $A$  is the cross sectional area,  $P$  is the perimeter and  $\Delta z$  is the CV length. The mean values over the CV used in equation (1) are defined as:

$$\begin{aligned} \tilde{\rho}_P &= \frac{1}{V_P} \int_{V_P} \rho dV \quad ; \quad \tilde{p}_P = \frac{1}{V_P} \int_{V_P} p dV \\ \bar{e}_P &= \frac{1}{\tilde{\rho}_P V_P} \int_{V_P} \rho e dV \quad ; \quad \bar{q}_P = \frac{1}{\Delta z_P} \int_{z_w}^{z_e} \dot{q} dz \end{aligned}$$

Transient terms are evaluated using a first order backward differencing scheme. Convective terms at the CV faces are evaluated using first or higher order schemes. When a first order scheme is used, the variables at a given face of the CV are taken equal to the nearest upstream nodal values (this is the upwind scheme). Higher order schemes, as Quick or Smart [15], are introduced using a deferred correction approach, i.e. the convective term is evaluated using the upwind scheme while an extra or correction term is introduced in the source term of the discretized equation keeping the diagonal dominance of the coefficient matrix. The convective heat flux is integrated along the CV heat transfer surface using local heat transfer coefficients and nodal temperatures for the inner tube and the refrigerant fluid.

Introducing all the above numerical schemes and models in the energy equation

and approximating mean quantities by their values of the central node, the following fully discretized form is obtained.

$$\begin{aligned} & (\rho_P e_P - \rho_P^o e_P^o) A \frac{\Delta z}{\Delta t} + \dot{m}_P^s e_e - \dot{m}_W^s e_w = \\ & \alpha_P (T_P^t - T_P^f) P \Delta z + (p_P - p_P^o) A \frac{\Delta z}{\Delta t} \end{aligned} \quad (2)$$

Equation (2) can be re-written in the generic discretized form  $a_P^h h_P = a_E^h h_E + a_W^h h_W + b_P^h$ , in terms of the enthalpy as:

$$\begin{aligned} a_W^h &= \max(\dot{m}_W^s, 0.0) \\ a_E^h &= \max(-\dot{m}_P^s, 0.0) \\ a_P^h &= a_E^h + a_W^h + \rho_P^o A \frac{\Delta z}{\Delta t} \\ b_P^h &= \left[ \rho_P^o h_P^o - \rho_P (e_{cP} + e_{pP}) + \rho_P^o (e_{cP}^o + e_{pP}^o) + (p_P - p_P^o) \right] A \frac{\Delta z}{\Delta t} - \\ & \quad \dot{m}_P^s [e_{ce} + e_{pe}] + \dot{m}_W^s [e_{cw} + e_{pw}] + \alpha_P (T_P^t - T_P^f) P \Delta z + \Delta conv \end{aligned} \quad (3)$$

High-order convective schemes are introduced through  $\Delta conv$  in the source term  $b_P^h$ . This quantity is evaluated from:

$$\begin{aligned} \Delta conv &= [\max(-\dot{m}_P^s, 0.0)(h_E - h_P) - \dot{m}_P^s (h_e^{ns} - h_P)] - \\ & \quad [\max(\dot{m}_W^s, 0.0)(h_W - h_P) + \dot{m}_W^s (h_w^{ns} - h_P)] \end{aligned}$$

where the variables  $h_e^{ns}$  and  $h_w^{ns}$  represent the fluid enthalpy at the CV faces itself evaluated by means of the selected high-order convective scheme. This is the deferred technique indicated above.

From the discretized energy equation, the nodal enthalpy  $h_P$  is obtained at each CV. Considering thermodynamic local equilibrium in the flow, the mass gas weight fraction  $x_{g,P}$  can be calculated in the two-phase flow zone as a function of the enthalpy  $h_P$  and the local pressure  $p_P$  as:  $x_{g,P} = [h_P -$

$h_l(p_P)]/[h_g(p_P) - h_l(p_P)]$ , where  $h_l$  and  $h_g$  represent the saturated liquid and gas enthalpies, respectively.

### *Momentum equation*

The momentum equation in the axial direction is discretized over the staggered volumes indicated in Figure 1b. In a semi-discretized form the momentum equation can be written as:

$$V \frac{\partial \bar{\rho} \bar{v}}{\partial t} + \dot{m}_{g,e^s} v_{g,e^s} + \dot{m}_{l,e^s} v_{l,e^s} - \dot{m}_{g,w^s} v_{g,w^s} - \dot{m}_{l,w^s} v_{l,w^s} = (p_P - p_E)A - \bar{\tau}_w P \Delta z - mg \sin \theta \quad (5)$$

Sub-indexes  $g$  and  $l$  indicate gas and liquid phase respectively. The gas mass flux  $\dot{m}_g$  and the liquid mass flux  $\dot{m}_l$  can be expressed as a function of the total mass flux of the refrigerant  $\dot{m}$  and the mass gas weight fraction  $x_g$  as:  $\dot{m}_g = x_g \dot{m}$  and  $\dot{m}_l = (1 - x_g) \dot{m}$ . The gas and liquid velocities are expressed as a function of the void fraction, in the following form:  $v_g = \dot{m} x_g / \rho_g \epsilon_g A$  and  $v_l = \dot{m} (1 - x_g) / \rho_l (1 - \epsilon_g) A$ . The mixture density can be expressed as:  $\rho = \epsilon_g \rho_g + (1 - \epsilon_g) \rho_l$ .

The local shear stress in the momentum equation (5) is obtained in terms of the friction factor,  $\tau_w = (f/4)(\dot{m}^2/2\rho A^2)$ . In the single-phase flow, the friction factor  $f$  is determined by means of empirical information, while the mass flux  $\dot{m}$  and the density  $\rho$  are evaluated depending on the phase flow present, gas or liquid. In case of two-phase flow, the shear stress is determined by means of the friction factor corresponding to the gas phase,  $f_g$ , the gas mass flux  $\dot{m}_g$ , the gas density  $\rho_g$  and the multiplier two-phase factor  $\Phi$ , as  $f = f_g \Phi$ . The friction factor and multiplier two-phase factor are empirically obtained.

Introducing in equation (5) the expressions commented above, and rearranging

according to the general form of momentum equation,  $a_P^v \dot{m}_{P^s} = a_E^v \dot{m}_{E^s} + a_W^v \dot{m}_{W^s} + b_P^v$ , the following discretized coefficients are obtained:

$$\begin{aligned}
 a_W^v &= \max(\dot{m}_{w^s}, 0.0) K_{w^s} \\
 a_E^v &= \max(-\dot{m}_{e^s}, 0.0) K_{e^s} \\
 a_P^v &= \max(\dot{m}_{e^s}, 0.0) K_{e^s} - \max(-\dot{m}_{w^s}, 0.0) K_{w^s} + \frac{f}{4} \left[ \frac{|\dot{m}_{P^s}|}{2\rho_{P^s} A^2} \right] P \Delta z + \frac{\Delta z}{\Delta t} \\
 b_P^v &= (p_P - p_E) A + \dot{m}_P^o \frac{\Delta z}{\Delta t} - \rho_{P^s} g \sin\theta A \Delta z + \Delta conv \\
 \Delta conv &= [\max(-\dot{m}_{e^s}, 0.0) \dot{m}_{j+1} - \max(\dot{m}_{e^s}, 0.0) \dot{m}_j - \dot{m}_e^{ns}] K_E - \\
 &\quad [\max(\dot{m}_{w^s}, 0.0) \dot{m}_{j-1} + \max(-\dot{m}_{w^s}, 0.0) \dot{m}_j - \dot{m}_w^{ns}] K_P
 \end{aligned} \tag{6}$$

where,  $K = [x_g^2 / \rho_g \epsilon_g A + (1 - x_g)^2 / \rho_l (1 - \epsilon_g) A]$ . This variable is evaluated at the node of the main mesh (in fact,  $K_{e^s} = K_E$  and  $K_{w^s} = K_P$ ). Using the Central Difference scheme (CDS) for the convective terms, the mass flux on the staggered volume faces are defined as:  $\dot{m}_{e^s} = (\dot{m}_{E^s} + \dot{m}_{P^s})/2$  and  $\dot{m}_{w^s} = (\dot{m}_{P^s} + \dot{m}_{W^s})/2$ , and density value over the CV center of the staggered mesh are defined as:  $\rho_{P^s} = (\rho_E + \rho_P)/2$ . The mass flux  $\dot{m}_e^{ns}$  and  $\dot{m}_w^{ns}$  are evaluated using the Quick or Smart numerical scheme in the deferred correction term  $\Delta conv$ .

#### *Pressure correction equation*

A pressure correction equation is evaluated over the main control volumes (Figure 1a) by means of the continuity equation and according to the SIMPLE method [14]. The strategy starts from the semi-discretized form of the continuity equation:

$$V_P \frac{\partial \tilde{\rho}_P}{\partial t} + \dot{m}_e - \dot{m}_w = 0 \tag{7}$$

The mass flow is estimated from the discretized momentum equation rewrit-

ten as:  $\dot{m}_e = \dot{m}_e^* + d_e^v(p'_P - p'_E)$  and  $\dot{m}_w = \dot{m}_w^* + d_w^v(p'_W - p'_P)$ , where  $\dot{m}_e^*$  and  $\dot{m}_w^*$  indicate the mass fluxes obtained from the momentum equation assuming a guess pressure field  $p^*$ . The variable  $p'_P$  represents the correction needed to verify the continuity equation. The coefficients  $d_e^v$  and  $d_w^v$  appear rearranging the discretized momentum equation (see [14] for details). Introducing the above expression of the cell face mass fluxes into equation (7), and approximating by their nodal value the mean CV quantities, the correction pressure equation can be written as:

$$\frac{\rho_P - \rho_P^o}{\Delta t} A \Delta z + [\dot{m}_{P^s}^* + d_e^v(p'_P - p'_E)] - [\dot{m}_{W^s}^* + d_w^v(p'_W - p'_P)] = 0 \quad (8)$$

This equation can be rewritten in terms of the generic discretized equation  $a_P^p p'_P = a_E^p p'_E + a_W^p p'_W + b_P^p$ , where the discretized coefficient can be easily obtained from equation (8). After pressure correction is obtained, the mass fluxes and pressure field are updated:  $\dot{m}_{P^s} = \dot{m}_{P^s}^* + \dot{m}'_{P^s}$  and  $p_P = p_P^* + p'_P$ .

## 2.2 Secondary fluid in the annulus region

The secondary fluid flows in the annulus area, defined between inner tube and outer tube. The mathematical formulation is similar to the one presented for the refrigerant fluid in the inner tube, except that heat transfer and wall friction between the fluid and both the inner tube and outer tube must be considered. In this work, only single-phase flow is considered to occur in the annulus region. The general SIMPLE algorithm described above can be used. However, if no complex flow is expected (e.g. no back flow phenomena), the step by step method can also be used. The method solves the governing equations at each CV, step by step in the flow direction (see [12] for details).

### 2.3 Heat conduction in solid elements

Three different solids are considered, the inner tube, the outer tube and the insulator. Details of the defined main control volumes (CVs) in the different parts of the heat exchanger are depicted in Figure 2. To solve the solid elements, the energy equation is applied over each CV. A general heat conduction equation can be integrated, obtaining the following generic form:

$$\rho c_p \frac{(T_P - T_P^o)}{\Delta t} V_P = \dot{Q}_w + \dot{Q}_e + \dot{Q}_n + \dot{Q}_s \quad (9)$$

where the left hand side indicates the internal energy increase in the CV, while the right hand represents the inlet net heat flux through the CV-faces (west, east, north, and south). Depending on which solid should be solved, the value of heat fluxes are different. For the inner tube the different heat fluxes through the CV-faces are the consequence of convective heat transfer with the refrigerant fluid and the secondary fluid, together with axial heat conduction through the tube itself. These fluxes can be approximated as:

$$\begin{aligned} \dot{Q}_w &= \lambda_w^t \left( \frac{T_W^t - T_P^t}{d_{PW}} \right) A_{t,in} \\ \dot{Q}_e &= \lambda_e^t \left( \frac{T_E^t - T_P^t}{d_{PE}} \right) A_{t,in} \\ \dot{Q}_s &= \alpha^f (T_P^f - T_P^t) \pi D_i \Delta z_P \\ \dot{Q}_n &= \alpha^{f.sec.o} (T_P^{f.sec} - T_P^t) \pi D_o \Delta z_P \end{aligned}$$

Where  $\alpha^f$  and  $\alpha^{f.sec.o}$  are the heat transfer coefficient of the refrigerant and the secondary fluid in the inner tube respectively,  $T_P^f$  is the refrigerant fluid temperature and  $T_P^{f.sec}$  is the secondary fluid temperature,  $d_{PW}$  and  $d_{PE}$  are the distance between nodes, and  $A_{t,in}$  is the cross-section,  $A_{t,in} = \pi(D_o^2 - D_i^2)/4$ .

For the outer tube, the secondary fluid is in contact with the tube at south face, while heat conduction is applied on the other CV's faces. Thus, the heat fluxes can be approximated as:

$$\begin{aligned}\dot{Q}_w &= \lambda_w^{t.out} \left( \frac{T_W^{t.out} - T_P^{t.out}}{d_{PW}} \right) A_{t.out} \\ \dot{Q}_e &= \lambda_e^{t.out} \left( \frac{T_E^{t.out} - T_P^{t.out}}{d_{PE}} \right) A_{t.out} \\ \dot{Q}_s &= \alpha^{f.sec.e} (T_P^{f.sec} - T_P^{t.out}) \pi D_e \Delta z_P \\ \dot{Q}_n &= \lambda_n \left( \frac{T_N^{t.ins} - T_P^{t.out}}{\Delta r_n} \right) \pi D'_e \Delta z_P\end{aligned}$$

where  $T^{t.out}$  and  $T^{t.ins}$  indicate the temperatures of the outer tube and insulator respectively. An harmonic mean thermal conductivity is used at the contact surface between the tube and the insulator,  $\lambda_n = d_{PN} [d_{PN}/\lambda_{wall} + d_{nN}/\lambda_{insulator}]^{-1}$ . This criterion is obtained as a consequence of the condition of heat flux continuity at the interface, and after approximating temperature gradients by a backward (in the tube) and forward (in the insulator) first-order numerical scheme.

For the insulator, the conduction heat fluxes through any of the internal CV-faces can be approximated as:

$$\begin{aligned}\dot{Q}_w &= \lambda_w^{ins} \left( \frac{T_W^{ins} - T_P^{ins}}{d_{PW}} \right) A_{ins} \\ \dot{Q}_e &= \lambda_e^{ins} \left( \frac{T_E^{ins} - T_P^{ins}}{d_{PE}} \right) A_{ins} \\ \dot{Q}_s &= \lambda_s^{ins} \left( \frac{T_S^{ins} - T_P^{ins}}{\Delta r_s} \right) \pi D_s \Delta z \\ \dot{Q}_n &= \lambda_n^{ins} \left( \frac{T_N^{ins} - T_P^{ins}}{\Delta r_n} \right) \pi D_n \Delta z\end{aligned}$$

The boundary conditions in the west and the east extreme nodes of the tubes and insulator can be a fix temperature or a null heat flux. Natural convection

with the ambient is considered in the external part of the insulator.

#### 2.4 Empirical information

The empirical information used to evaluate the local heat transfer coefficients  $\alpha$  and the friction factors  $f$  in single-phase and two phases, together with the void fraction  $\epsilon_g$  are presented.

The single-phase heat transfer coefficient is obtained for laminar and turbulent regimes using Nusselt and Gnieliski correlations respectively [16]. The friction factor is evaluated from Churchill expression [16].

In case of condensation, the heat transfer coefficient is evaluated with Shah [17] correlation. Even though Shah's correlation is defined for annular flow, the expression is used along the flow. The empirical correlation given by Shah is available for gas weight fraction between 0.15 and 0.85. For the rest of the range there is no data available. In this case, two splines functions between single-phase and two-phase heat transfer correlations and vice-versa have been obtained for three-order polynomial equations considering continuity and derivability in the functions. The first one is ranged between 0.0 and 0.15, while the second one is ranged between 0.85 to 1.0. The spline coefficients are function of Re, Pr, duct geometry and fluid thermodynamic properties.

Three sub-zones are presented in tube evaporation in the two-phase flow region. These sub-zones are: sub-cooled boiling, saturated boiling and dry-out. The heat transfer coefficient during evaporation may be evaluated using different correlations depending on which sub-zone the flow is located.

Different correlations have been tested in the evaporation zone. The heat transfer coefficient in the sub-cooled zone is determined by Forster and Zuber correlation [16] or by Kandlikar correlation [18]. These correlations are used when

the wall temperature at a given location is equal to or greater than the local saturation temperature. The heat transfer for the saturated zone can be evaluated by means of the Shah correlation for evaporation [19], Kandlikar for saturated flow boiling [20], or Kattan et al. evaporation model [21]. The heat transfer coefficient in the dry-out zone can be obtained using Kattan et al. [22][23] or Groeneveld [24] correlations. The Groeneveld correlation needs to determinate a previous point where the dry-out condition begins. The Kattan et al. [22] correlation estimates and recognizes the dry-out point by means of the evaporation flow pattern maps.

The Kandlikar correlations for sub-cooling boiling [18] and saturated flow boiling [20] do not present any discontinuity if both are used together. In this case, it is only necessary to take into account the transition zone from saturated boiling to dry-out, where Kattan et al. [22][23] or Groeneveld [24] correlations can be used.

The Shah correlation for evaporation [19] is only available in the saturation boiling zone. Therefore, splines functions between single-phase and two-phase phenomena are needed.

A more complete description of the heat transfer boiling phenomena is presented by Kattan et al. [21][22][23], which gives the value of heat transfer coefficient in saturation boiling and post dry-out zones.

The void fraction is calculated from the semi-empirical Premoli's equation [25]. The shear stress in condensation and evaporation is calculated from the Jung and Radermacher [26] or Friedel [27] correlations.

All thermodynamic properties are iteratively evaluated at each local position by means of the REFPROP program [28], as function of the local pressure and enthalpy.

### 3 NUMERICAL RESOLUTION

This section presents the numerical resolution of the whole double-pipe heat exchanger. The global numerical algorithm takes into account, in a coupled manner, the thermal and fluid dynamical behaviour of the different elements of the system: i) the two-phase fluid flow in the inner tube (condensation and evaporation phenomena), ii) the single-phase flow in the annulus area, iii) the heat conduction through the solid elements (the inner tube, the outer tube and the insulator). Subsection 3.1 shows the global algorithm and the interactions between fluids and solids. Subsection 3.2 presents the initial and boundary conditions required by the numerical method. Finally, subsection 3.3 shows the phase change transition criteria used in the solution of single and two-phase flow.

#### 3.1 Numerical algorithm

The whole heat exchanger has been solved by means of a segregated fully implicit numerical scheme following the algorithm presented in Figure 3. The refrigerant inner fluid is solved using the general SIMPLE method [14] (see detail in section 2.1) to take into account the possibility of complex flow phenomena in the refrigeration system. The secondary fluid can be solved using the SIMPLE method described in this paper. However, the step by step method described in reference [12] or [13] is preferred when no back flow is expected. The temperature in the inner tube and in the outer tube and insulator are calculated using the discretized heat conduction equation (9).

The convergence of the different iterative loops is based on the maximum difference between the different local variables at the previous iteration  $\phi^*$  and at the actual one  $\phi$ , i.e.  $\max|\phi^* - \phi|/\phi < \delta$ , where  $\delta$  is the convergence

criteria. The process runs step-by-step in the time direction until some criteria is satisfied (e.g. steady-state conditions are reached, or just after some physical period of time).

### 3.2 Initial and boundary conditions

At the initial instant ( $t=0$ ), pressure, mass flux and enthalpy distribution of the refrigerant and secondary fluids must be fully specified, together with temperatures in the solid elements.

For the refrigerant fluid in the inner tube, the SIMPLE method [14] solves the coupled governing equations considering the desired steady or unsteady boundary conditions, and allowing back flow phenomena if it is produced. For the secondary fluid, the SIMPLE method or step by step method can be used (no back flow phenomena is considered in this case). Two main boundary conditions can be used: i) the inlet mass flux  $\dot{m}_{in}$ , the inlet enthalpy  $h_{in}$ , and the outlet pressure  $p_{out}$ , or ii) the inlet pressure  $p_{in}$ , the inlet enthalpy  $h_{in}$ , and the outlet pressure  $p_{out}$ . The use of other boundary conditions are also possible.

For the solid elements, adiabatic boundary conditions are imposed at the lateral boundaries ( $z=0$  and  $z=L$ ). Pressure and temperature ambient conditions must also be given.

### 3.3 Phase change criteria for the refrigerant fluid

The transition criteria between the three main zones existing in both condensation and evaporation processes are evaluated depending on fluid enthalpy. These condition are: i) liquid region: the value of the enthalpy  $h_P$  over the control volume is lower than the liquid saturation enthalpy  $h_{l,sat}$  at local con-

ditions; ii) two-phase region: the enthalpy  $h_P$  over the control volume is greater than the local liquid saturation enthalpy  $h_{l,sat}$  but lower than the gas saturation enthalpy  $h_{g,sat}$ ; iii) gas region: the enthalpy  $h_P$  over the control volume is greater than the local gas saturation enthalpy  $h_{g,sat}$ .

The evaporation processes have two sub-zones or subregions: sub-cooled boiling and dry-out. The sub-cooled boiling criteria begins when the fluid enthalpy  $h_P$  is lower than the liquid saturation enthalpy  $h_{l,sat}$  and the wall temperature  $T^t$  is greater than the saturation temperature of fluid  $T_{sat}^f$ . The dry-out criteria begins when the fluid enthalpy  $h_P$  is lower than the gas saturation enthalpy  $h_{g,sat}$ , but is greater than the liquid saturation enthalpy, and gas weight fraction  $x_g$  is greater than gas weight fraction  $x_{g,do}$  at dry-out conditions. Using the previous criteria at each control volume is possible to define the proper zone.

#### 4 NUMERICAL VERIFICATION

This section shows the quality of the numerical solutions by means of a critical analysis of the different numerical sources of computational errors: convergence errors and discretization errors.

Two cases of two-phase flow of R134a inside a tube with specified heat flux at the wall are selected. The first one corresponds to a evaporation case inside a tube of 3 m of length and 9.10 mm of inner diameter. The refrigerant is evaporated with a constant heat flux through the tube walls of 10000 W/m<sup>2</sup>. The pressure, mass flux and flow conditions at the inlet section (z=0) are 4.146·10<sup>5</sup> Pa, 0.0226 kg/s and 230.0 kJ/kg, respectively.

The second case corresponds to a condensation process inside a tube with the same geometry as the one indicated above. The refrigerant is condensed with

a constant extraction of the heat flux of  $49000 \text{ W/m}^2$ . The pressure, mass flux and flow conditions at the inlet section ( $z=0$ ) are  $1.047 \cdot 10^6 \text{ Pa}$ ,  $0.0201 \text{ kg/s}$  and  $445.0 \text{ kJ/kg}$ , respectively.

Results obtained for both cases, evaporation and condensation considering different convergence criteria and number of CVs, are shown in Table 1. The values of temperature and enthalpy of the refrigerant fluid at the exit ( $z=L$ ) are presented in both cases. Numerical results tend to give an asymptotic solution when the grid is refined enough and when the convergence criteria is sufficiently low. A reference numerical solution is found for 2800 CVs and  $10^{-12}$  as convergence criteria.

The influence of the convergence criteria is analysed changing its value from  $10^{-6}$  to  $10^{-12}$  and using 2800 CVs. Differences between  $10^{-6}$  and  $10^{-12}$  give a maximum discrepancies of 0.0721% and 2.759% in enthalpy and temperature for the evaporation case. However, when the convergence criteria is  $10^{-10}$  the discrepancies between the obtained results and the reference solution are insignificant. The influence of the number of CVs is also evaluated. The condensation case gives higher discrepancies between results obtained with different number of CVs. Eg., for 20, 50, 200 and 800 CVs, the discrepancies in temperature (in comparison with reference solution) has been 64.88%, 21.46%, 0.68% and 0.062%, respectively. See Table 1 for details.

In order to show the influence of the different numerical schemes, Figure 4 depicts an illustrative condensation case considering Upwind, Quick and Smart schemes. The condensation occurs inside a tube with 2 m of length and 6.0 mm of inner diameter. The refrigerant R134a is condensed with a constant extraction of the heat flux of  $14000 \text{ W/m}^2$ . The inlet conditions ( $z=0$ ) correspond to the gas phase at the following pressure, mass flux and enthalpy values:  $1.496 \cdot 10^6 \text{ Pa}$ ,  $0.00338 \text{ kg/s}$  and  $464.7 \text{ kJ/kg}$ , respectively. The results are obtained with two different grid numbers, 20 CVs and 2000 CVs, and a

convergence criteria of  $10^{-12}$ . The results obtained with 2000 CVs correspond to the reference grid independent solution.

The numerical comparative results of the fluid temperature at the exit section ( $z=L$ ) between the three different numerical schemes used in the solution are presented for two different grid numbers. Results obtained for 20 CVs ( $40.425^{\circ}C$ ,  $40.135^{\circ}C$  and  $40.135^{\circ}C$ ) in comparison with the reference solution ( $39.573^{\circ}C$ ), present errors of 2.15%, 1.42% and 1.42% when Upwind, Quick and Smart schemes are applied, respectively. Difference not only affects the fluid temperature at outlet, but also along all condenser length (see details in Figure 4).

## 5 EXPERIMENTAL COMPARISON

After the verification of the numerical solution is completed, an experimental comparison is carried out. The objective of this comparison is to validate the mathematical model developed. The experimental data have been obtained from the scientific literature considering different fluid refrigerants, geometries and both condensation and evaporation phenomena. The comparative study is focused on two condensation and two evaporation cases.

### 5.1 *Condensation*

The numerical simulation of condensation process considers the adapted treatment of the heat transfer coefficient correlations detailed above. Between single gas phase and condensation the first spline function is used, while between the final step of condensation and single liquid phase the second one is applied.

Figure 5 depicts the values of the local heat transfer coefficient, the wall and

fluid temperatures during condensation processes inside a tube with 2 m of length and 6.0 mm of inner diameter. The refrigerant R134a is condensed with a constant extraction of a heat flux of  $14000 \text{ W/m}^2$ . The pressure, mass flux and flow conditions at the inlet section ( $z=0$ ) are  $1.496 \cdot 10^6 \text{ Pa}$ ,  $0.00338 \text{ kg/s}$  and  $464.7 \text{ kJ/kg}$ , respectively. In this case, the splines are used (adapted correlations) based on the available correlation from the literature. The influence of the heat transfer coefficient adapted over the wall temperature is shown in the jump wall temperature from single-phase to two-phase. The fluid temperature obtained with the adapted treatment shows significant differences in comparison with the not adapted one. A comparison between experimental and numerical value of the fluid temperature at the outlet section has been made. Discrepancies of 0.90% and 6.02% for adapted and not adapted treatment respectively have been obtained.

Using the adapted treatment for the empirical correlations, the experimental validation is performed by means of the comparison between the numerical results and the experimental data Cavallini et al. [29], who reported experimental heat transfer coefficients and pressure drop for condensation inside tubes and considering different refrigerants. Specific cases of condensation inside a tube of 8 mm diameter with mass flux of 200, 400 and  $750 \text{ kg/m}^2\text{s}$  for refrigerants R134a and R22 are depicted in Figure 6.

In the R134a condensation case, and for mass fluxes between 400 and  $750 \text{ kg/m}^2\text{s}$  the agreement between numerical results and experimental data are quite good. However, for mass flux of  $200 \text{ kg/m}^2\text{s}$ , the numerical results under-predict the experimental data at low mass fractions. In the R22 condensation case, the numerical and experimental results present a similar behaviour, although the heat transfer coefficient is slightly over-predicted at high mass fluxes and under-predicted at low mass fluxes.

The numerical results with the adapted treatment of correlations do not pro-

duce abrupt alterations in the value of the local heat transfer coefficient or in the value of the wall temperature. The adapted treatment procedure gives stability to the numerical resolution process and does not allow discontinuities during the evaluation of the heat transfer.

## 5.2 Evaporation

Two validation cases in the evaporation process are presented, Jung and Didion [30] and Kattan et al. [23] cases. Jung and Didion reported experimental data of the wall temperature, fluid temperature and pressure. The wall temperature reported is located on the top, bottom, right and left of the tube. A tube of 9 mm of diameter is used in this experiment. The refrigerant R22 is evaporated with a constant heat flux of  $10060 \text{ W/m}^2$  across the tube. The refrigerant has a mass flux of  $500 \text{ kg/m}^2\text{s}$  with an inlet pressure of  $4.05 \cdot 10^5 \text{ Pa}$  and an inlet enthalpy of  $185 \text{ kJ/kg}$ .

The numerical results and experimental data are depicted in Figures 7 and 8. The heat transfer coefficient has different behaviour depending on the correlations used. Figure 7a shows the heat transfer coefficient calculated by means of the Kandlikar correlation, and also the Shah correlation (with and without adapted treatment).

For the pressure distribution, the numerical results and the experimental data are shown in Figure 7b. The numerical model gives results similar to the experimental data. The measured pressure displays a large decrease at the middle of the tube, attributed to the experimental setup (see [30] for details).

The influence of the adapted and non-adapted heat transfer coefficient on the wall temperature is depicted in Figure 8a. The wall temperature is abruptly changed between the sub-cooled boiling and the two-phase zones if the adapted

treatment is not employed. When both Kandlikar sub-cooled [18] and saturated [20] correlations are used, the wall temperature does not suffer the abrupt changes indicated above and a more appropriate behaviour of the wall temperature is found. The aim of the Figure 8a is to show the influence of the transition zones treatment in the wall temperature. In this specific test case, the adapted Shah correlation gives better results than the adapted Kandlikar correlation. Both correlations predict similar fluid temperature distributions which agrees quite well with the experimental data as shown in Figure 8b.

Kattan et al. [21] report the heat transfer coefficient in their experimental results for evaporation of R134a. The evaporation occurs at 10 °C of saturated temperature inside a 12 mm diameter tube and a mass flux of 200 kg/m<sup>2</sup>s. A constant heat flux of 10000 W/m<sup>2</sup> is applied to the tube.

The comparison between the numerical simulation and the experimental of heat transfer coefficient is depicted in Figure 9. The numerical results display the correct trend in the heat transfer coefficient, even though the transition between the boiling zone and the dry-out zone is difficult to model, due to the sharp decrease of the heat transfer coefficient. However, using the Kattan correlation and employing the differentiation between regions, the post-dryout zone is predicted correctly.

## 6 ILLUSTRATIVE RESULTS

A group of different cases using a double-pipe heat exchanger and considering evaporation and condensation processes have been analysed. Fourteen cases are simulated, seven of these belong to a double-pipe evaporator and the other seven belong to a double-pipe condenser. The comparison between the numerical results and the experimental data of the refrigerant and secondary fluids temperatures at outlet are depicted in Figure 10.

Experimental data are obtained from an experimental unit (see [31] for details). The double-pipe evaporator consists in two concentric tubes of 6 m length, the internal diameters of the inner tube is 8.15 mm and the outer tube is 16.0 mm. The double-pipe condenser has 2 m length and the diameters of tubes are the same as the evaporator.

The conditions of the refrigerant fluid (R134a) at the inlet for the evaporation cases range between the following values: mass flux from 0.00115 to 0.00538 kg/s, pressure from  $1.34 \cdot 10^5$  to  $3.91 \cdot 10^5$  Pa, and temperature from  $-19.72$  to  $8.30^\circ\text{C}$ . In the same form, the conditions of the secondary fluid (water) at the inlet are between the next range: mass flux from 0.033 to 0.035 kg/s, pressure of  $2 \cdot 10^5$  Pa and temperature from 25.75 to  $31.4^\circ\text{C}$ .

The conditions of the refrigerant fluid (R134a) at the inlet for the condensation cases are between the next range of values: mass flux from 0.00115 to 0.00538 kg/s, pressure from  $14.64 \cdot 10^5$  to  $15.82 \cdot 10^5$  Pa, and temperature from 56.65 to  $95.25^\circ\text{C}$ . In the same form, the conditions of the secondary fluid (water) at the inlet are between the next range: mass flux from 0.025 to 0.031 kg/s, pressure of  $2 \cdot 10^5$  Pa and temperature from 25.0 to  $27.0^\circ\text{C}$ .

The comparison depicted in Figure 10 shows how the numerical results have a good agreement with the experimental data, presenting discrepancies lower of  $\pm 10\%$  in all cases.

## 7 CONCLUSIONS

A numerical model for analysing the condensation and evaporation phenomena inside ducts in double-pipe heat exchangers has been presented. The solution is obtained following a segregated numerical algorithm, where refrigerant inner fluid, secondary outer fluid and solid elements are iteratively solved.

The numerical simulation of two-phase flow is performed using the SIMPLE method with different numerical schemes for the convective terms: Upwind, Quick and Smart. The step by step method is applied to the secondary fluid in the annular region. Empirical information is needed in order to evaluate shear stress, heat flux and two-phase flow structure. The solid elements have been calculated solving the discretized conduction equation.

A numerical verification of the mathematical model is presented. The quality of the numerical solution has been assessed by means of a critical analysis of the different numerical sources of error (mainly convergence error and discretization error). The results clearly show the influence of different numerical parameters: convergence criteria, number of grid nodes, numerical schemes, etc. in order to obtain solutions not dependent of the numerical parameters chosen.

An experimental validation is also performed for different condensation and evaporation cases inside tubes. The comparative results between numerical model and experimental data present a reasonable good agreement. This agreement is also improved when the adapted treatment for the heat transfer coefficient correlation in the transition zones is considered. Furthermore, a more realistic behaviour of the wall temperature distribution is obtained by means of these criteria in comparison with non-adapted treatment in both condensation and evaporation phenomena. The method also improves the convergence characteristics of the numerical process. Illustrative results of double-pipe condenser and evaporator are also presented showing good agreement between numerical model and experimental data.

*Acknowledgement*

The authors gratefully acknowledge the financial support provided by the Spanish Government “Ministerio de Educación y Ciencia, Secretaría de Estado de Univesidades e Investigación” (ref. n<sup>o</sup>. ENE2005-08302), and the European Commission (ref. COOP-CT-No. 513106-EFROST).

ACCEPTED MANUSCRIPT

## NOMENCLATURE

A cross section area of the flux ( $m^2$ )

$A_t$  cross section area in the tube ( $m^2$ )

D diameter ( $m$ )

CV control volume

$c_p$  heat capacity ( $J kg^{-1}K^{-1}$ )

$d_{PE}$  distance between nodes P and E

$d_{PW}$  distance between nodes P and W

$e$  specific total energy ( $J kg^{-1}$ )

$e_c$  specific kinetic energy ( $J kg^{-1}$ )

$e_p$  specific potential energy ( $J kg^{-1}$ )

f friction factor

g acceleration of gravity ( $m s^{-2}$ )

h specific enthalpy ( $J kg^{-1}$ )

L length of heat exchanger ( $m$ )

$\dot{m}$  mass flow rate ( $kg s^{-1}$ )

m mass ( $kg$ )

P perimeter ( $m$ )

p pressure ( $Pa$ )

$\dot{Q}$  heat flux ( $W$ )

$\dot{q}$  heat flux per unit area ( $W m^{-2}$ )

$T$  temperature ( $^{\circ}C$ )

$V$  volume ( $m^3$ )

$v$  velocity ( $m s^{-1}$ )

$x_g$  gas weight fraction

$\alpha$  superficial heat transfer coefficient ( $W m^{-2} K^{-1}$ )

$\Delta t$  time step ( $s$ )

$\Delta z$  length of control volume ( $m$ )

$\delta$  rate of convergence

$\epsilon_g$  void fraction

$\lambda$  thermal conductivity ( $W m^{-1} K^{-1}$ )

$\rho$  density ( $kg m^{-3}$ )

$\tau_w$  wall shear stress ( $N m^{-2}$ )

$\theta$  inclination degree

#### Superscripts

f refrigerant fluid

f.sec secondary fluid

ins insulator

t inner tube

t.out outer tube

Subscripts

do dryout condition

g gas or vapour

l liquid

e,w,n,s east, west, north and south CV-faces

P main grid node associated to main CVs

E,W,N,S nearest east, west, north and south nodes associated to main grid  
node P

sat saturation condition

**References**

- [1] S. Kakac, H. Liu and K. Kakag, Heat exchangers: selection, rating and thermal design, CRC Press, 2002.
- [2] S. Levy, Two-phase flow in complex system, Wiley-Interscience Publications, New York, 1999.
- [3] G. B. Wallis, One-dimensional two-phase Flow, McGraw-Hill Book Company, New York, 1969.
- [4] G. Yadigaroglu and R.T. Lahey, On the various forms of the conservation equations in two-phase flow, International Journal of Multiphase Flow, Vol. 2, pp.477-494, 1976.
- [5] M. Ishi and T. Hibiki, Thermo-fluid dynamics of two-phase flow, Springer, New York, 2006.
- [6] A. Zavala-Rio and R. Santiesteban-Cos, Reliable compartmental models for double-pipe heat exchangers: An analytical study, Applied Mathematical Modelling, Vol. 31, pp. 1739-1752, 2007.
- [7] M. A. Abdelghani-Idrissi and F. Bagui, Countercurrent double-pipe heat exchanger subjected to flow-rate step change, Part I: New steady-state formulation, Heat transfer Engineering, 23, pp.4-11, 2002.
- [8] M. R. Ansari, and V. Mortazavi, Transient response of a co-current heat exchanger to an inlet temperature variation with time using an analytical and numerical solution, Numerical Heat Transfer, Part A, 52, pp.71-85, 2007
- [9] T. J. Rennie and G.S.V Raghavan, Numerical studies of double-pipe helical heat exchanger, Applied Thermal Engineering, Vol. 26, pp.1266-1273, 2006.
- [10] C.C. Wang, A numerical method for thermally non-equilibrium condensing flow in a double-pipe condenser, Applied Thermal Engineering, Vol. 17, N. 7, pp. 647-660, 1997.

- [11] W. Sripattrapan, T. Wongchang and S. Wongwises, Heat transfer and two-phase flow characteristics of refrigerants flowing under varied heat flux in double-pipe evaporator, *Heat and Mass Transfer*, Vol. 40, pp. 653-664, 2004.
- [12] F. Escanes, C.D. Pérez and A. Oliva, Thermal and fluid-dynamic behaviour of double-pipe condenser and evaporators - A numerical study, *Int. J. Num. Meth. Heat Fluid Flow*, vol. 5, pp. 781-795, 1995.
- [13] O. García, C.D. Pérez and J. Rigola, Numerical simulation of double pipe condensers and evaporators, *Int. Journal of Refrigeration*, vol. 27, Issue 6, pp 656-670, 2004.
- [14] S.V. Patankar, *Numerical heat transfer and fluid flow*, McGraw-Hill, NY, 1980.
- [15] M. S. Darwish and F.H. Moukalled, Normalized variable and space formulation methodology for high-resolution schemes, *Numerical Heat Transfer, Part B*, 26, pp.79-96, 1994.
- [16] G.F. Hewitt, *HEDH Heat Exchanger Design Handbook*, vol. 2, Begell House, Inc., New York, 2002.
- [17] M.M. Shah, A General Correlations for heat transfer during film condensation inside pipes, *Int. Journal Heat Mass Transfer*, vol. 22, pp. 547-556, 1979.
- [18] S.G. Kandlikar, Development of a flow boiling map for subcooled and saturated flow boiling of different fluid inside circular tubes, *Journal of Heat Transfer*, vol. 113, pp.190-200, February 1991.
- [19] M.M. Shah, Chart correlation for saturated boiling heat transfer: equations and further study, *ASHRAE Transaction No. 88*, 1982.
- [20] S.G. Kandlikar, Heat transfer characteristics in partial boiling, fully developed boiling and significant void flow regions of subcooled flow boiling, *Journal of Heat Transfer*, vol. 120, pp. 395-399, May 1998.
- [21] N. Kattan, J.R. Thome and D. Fravrat, Flow boiling in horizontal tubes: Part I - Development of a diabatic two-phase flow pattern map, *Journal of Heat Transfer*, vol. 120, pp. 140-147, February, 1998.

- [22] N. Kattan, J.R. Thome and D. Fravrat, Flow boiling in horizontal tubes: Part II - New heat transfer data for five refrigerants, *Journal of Heat Transfer*, vol. 120, pp. 148-155, February, 1998.
- [23] N. Kattan, J.R. Thome and D. Fravrat, Flow boiling in horizontal tubes: Part III - Development of a new heat transfer model based on flow pattern, *Journal of Heat Transfer*, vol. 120, pp. 156-165, February, 1998.
- [24] D.C. Groeneveld, Post-dryout transfer at reactor operating conditions, ANS Conference No. 730304, pp. 321-350, 1973.
- [25] C.K. Rice, The effect of void fraction correlation and heat flux assumption on refrigerant charge inventory predictions, *ASHRAE Transaction*, vol.93, pp. 341-367, 1987.
- [26] D.S. Jung and R. Radermacher, Prediction heat transfer coefficient and pressure drop of refrigerant mixtures in horizontal tubes, *Int. Journal of Refrigeration*, vol. 16, No. 3, pp. 201-209, 1993.
- [27] F. Friedel, Improved friction pressure drop correlation for horizontal and vertical two-phase pipe flow, *European Two-Phase Flow Group Meeting*, Paper E2, Ispra, Italy. 1979.
- [28] REPROP v7.0 Thermodynamic properties of refrigerants and refrigerants mixtures database. Standard Reference Database 23, USA. 2002.
- [29] A. Cavallini, G. Censi, D. Del Col, L. Doretti, G.A. Longo and L. Rossetto, Experimental investigation on condensation heat transfer and pressure drop of new HFC refrigerants (R134a, R125, R32, R410A R236ea) in a horizontal smooth tube, *Int. Journal of Refrigeration*, vol. 24, pp. 73-87, 2001.
- [30] D.S. Jung and A. Didion, Electrical Power Research Institute (EPRI) ER-6364, Research Project 8006-2, 1989.
- [31] J. Rigola, C.D. Pérez, O. García, J.M. Serra, M. Escribá and J. Pons, Numerical study and experimental validation of a complete vapor compression refrigerating cycle, *International compressor engineering conference*, pp. 201-206, Purdue University, Indiana, USA, 1998.

Table 1

Numerical study of SIMPLE method

Convergence criteria	Condensation		Evaporation	
	$h_{out}$	$T_{out}$	$h_{out}$	$T_{out}$
	(kJ/kg)	(°C)	(kJ/kg)	(°C)
$10^{-6}$	224.36	17.747	409.826	11.878
$10^{-8}$	224.39	17.766	410.123	12.216
$10^{-10}$	224.39	17.766	410.122	12.215
$10^{-12}$	224.39	17.766	410.122	12.215

Grid Number	Condensation		Evaporation	
	$h_{out}$	$T_{out}$	$h_{out}$	$T_{out}$
	(kJ/kg)	(°C)	(kJ/kg)	(°C)
20	208.57	6.243	410.102	12.192
50	219.10	13.952	410.111	12.203
100	223.77	17.321	410.116	12.208
200	224.22	17.645	410.115	12.208
400	224.33	17.728	410.121	12.214
800	224.37	17.755	410.121	12.210
1600	224.38	17.765	410.122	12.214
2000	224.39	17.766	410.122	12.215
2800	224.39	17.766	410.122	12.215

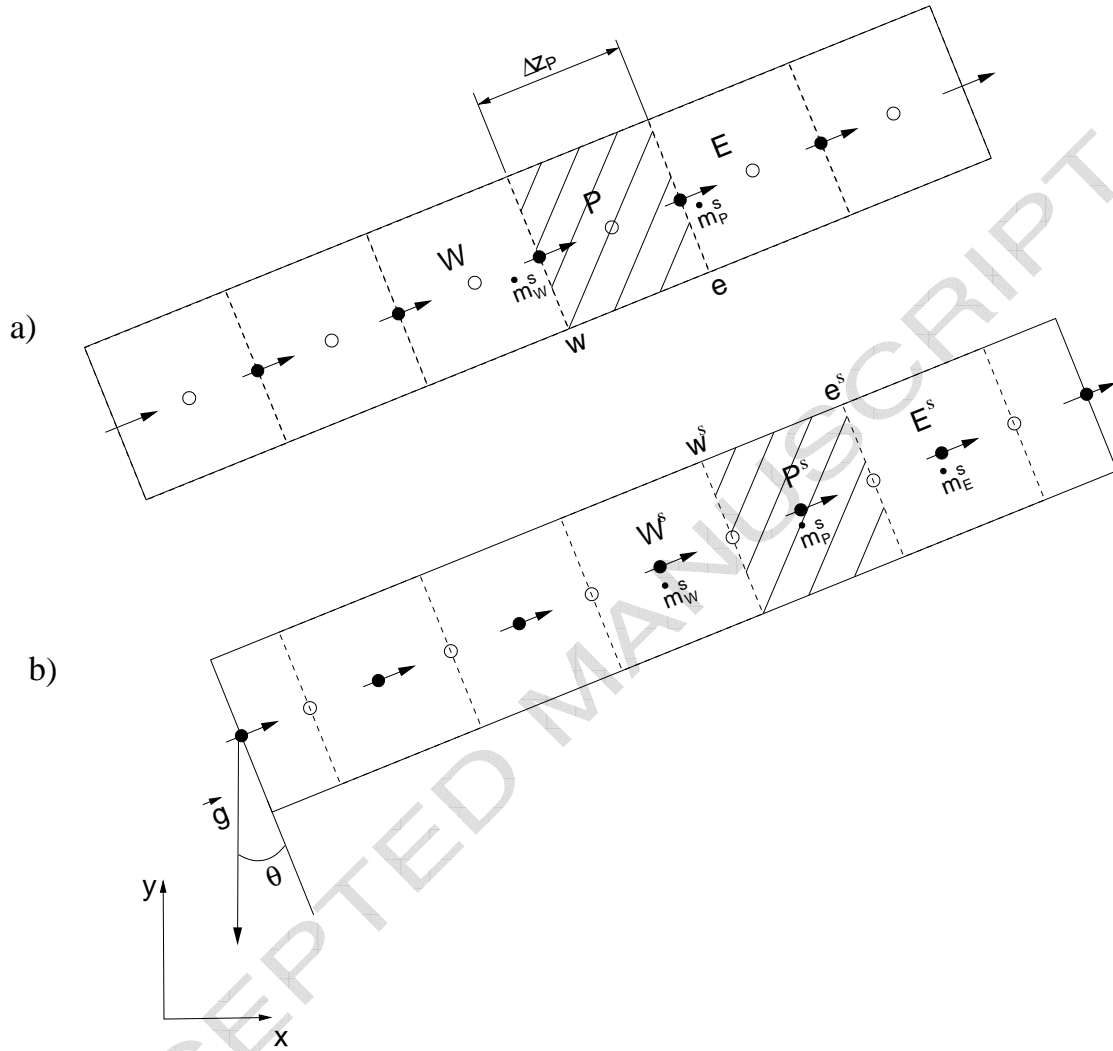


Fig. 1. Schematic representation of the meshes used in the discretization of the fluid flow: a) Main control volumes for pressure and energy, b) Staggered control volumes for mass flux. Symbol (o) indicates the node of the main mesh, and (•) indicates the node of the staggered mesh.

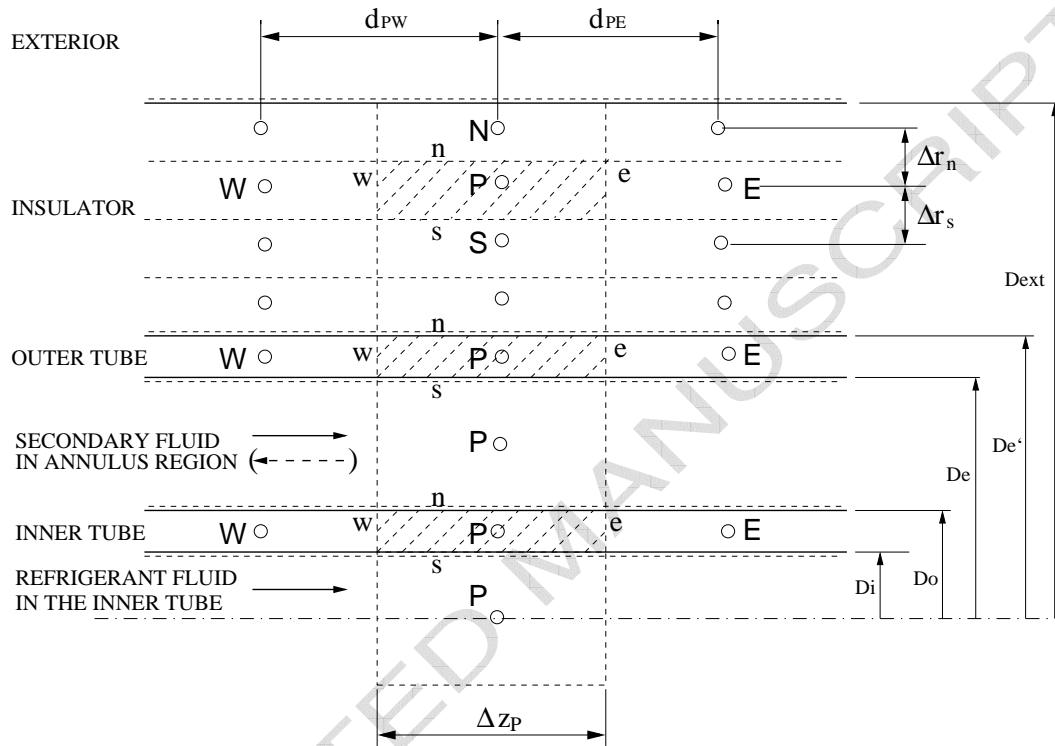


Fig. 2. Discretization of the solid elements and fluids. Main nodes assigned to the selected CVs are denoted by P, while W,E,N,S indicated their neighbours. Cell-faces are denoted by lower-case letters (w,e,n,s).

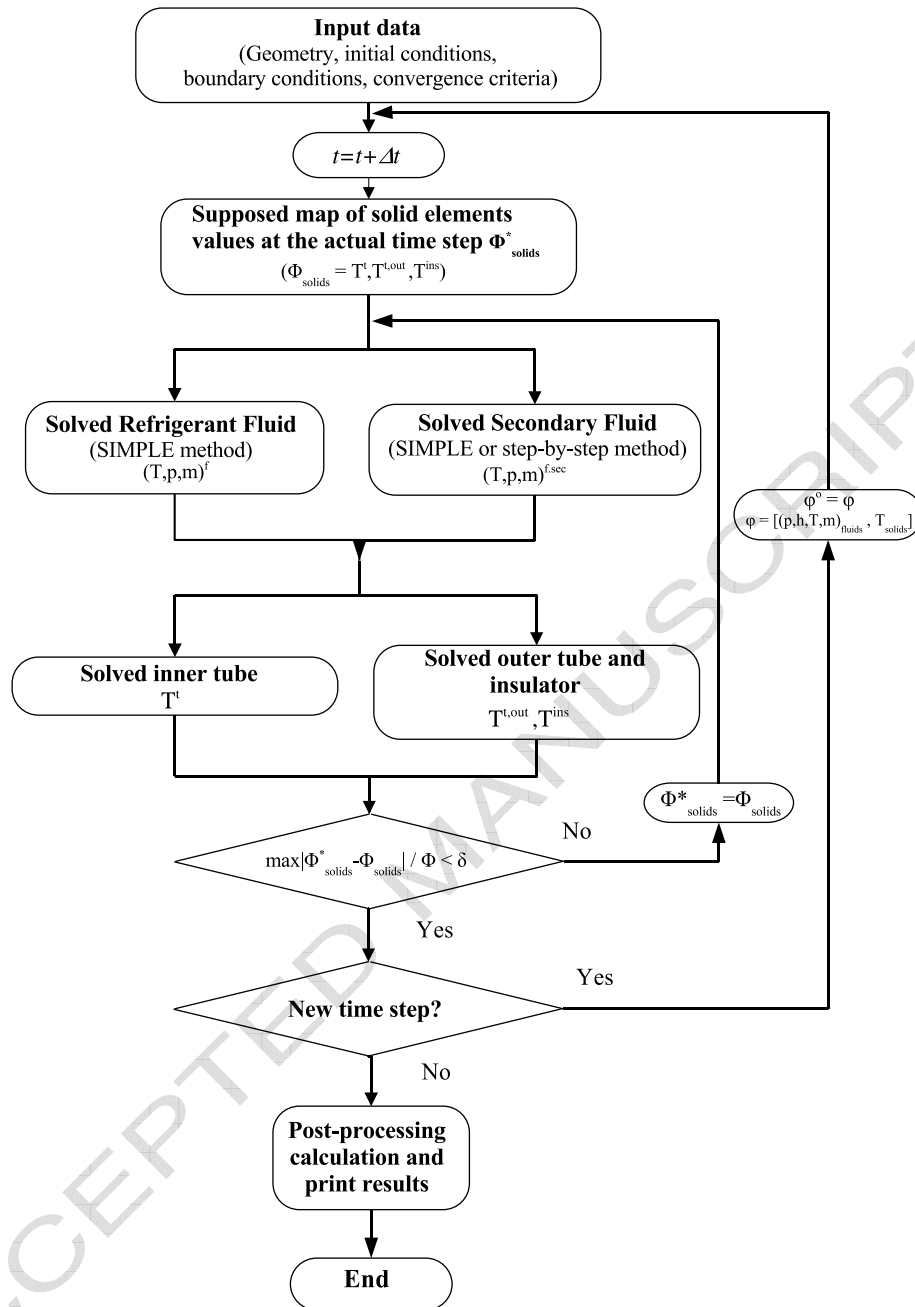


Fig. 3. Global numerical algorithm

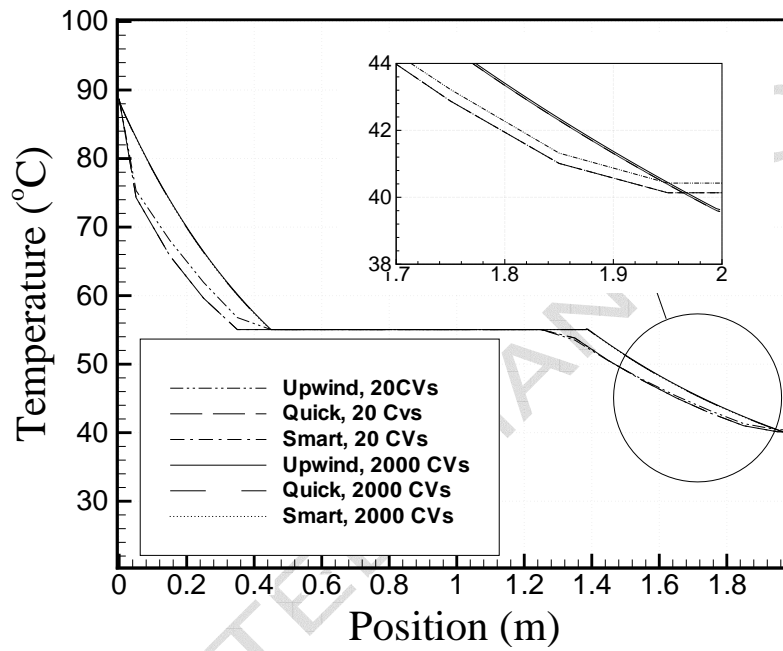


Fig. 4. Comparison of the numerical solution using SIMPLE method depending on the convective scheme for 20 CVs and 2000 CVs.

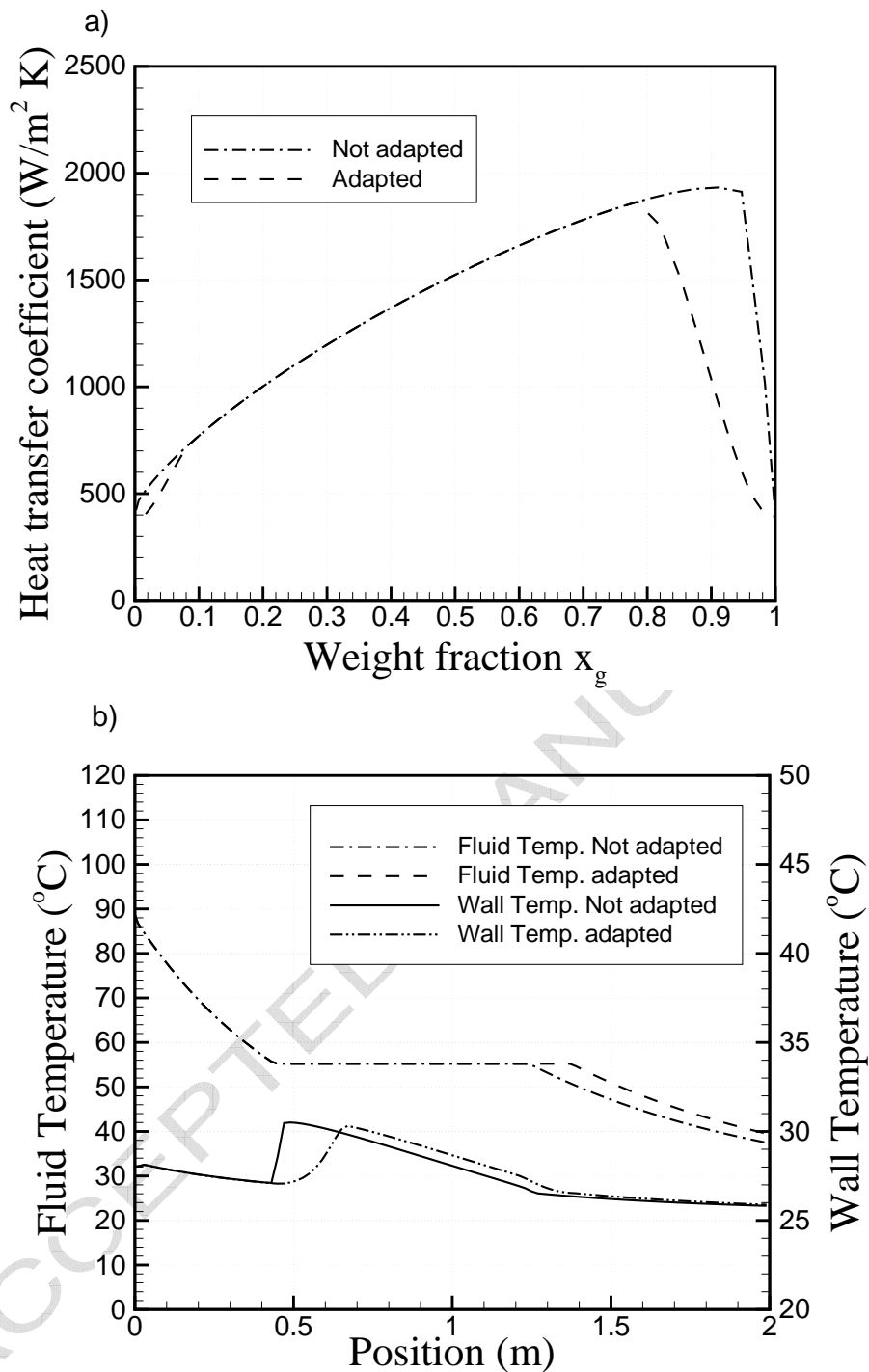


Fig. 5. Comparison between the numerical solution for adapted treatment correlation and not adapted in condensation, using Shah's correlation [17]: a) local heat transfer coefficient; b) temperatures.

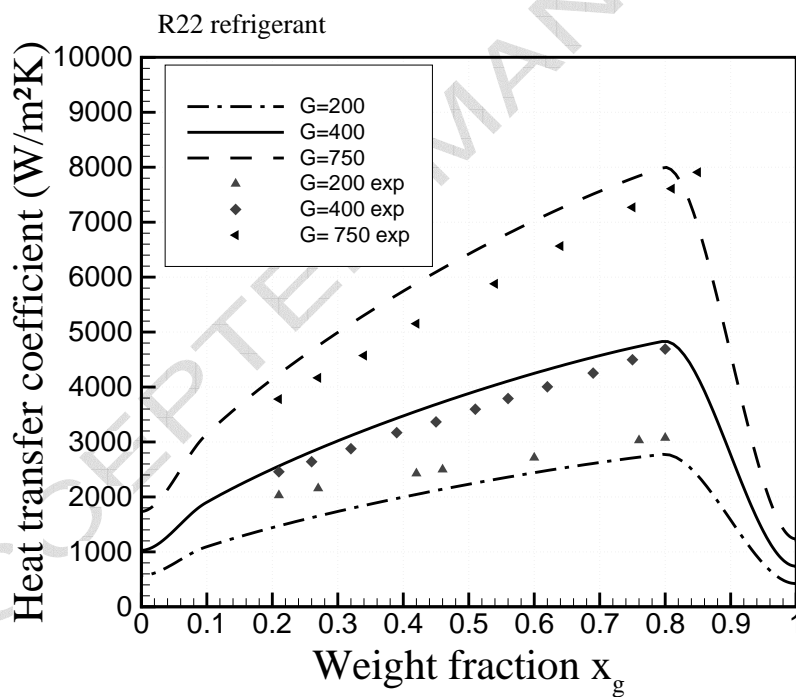
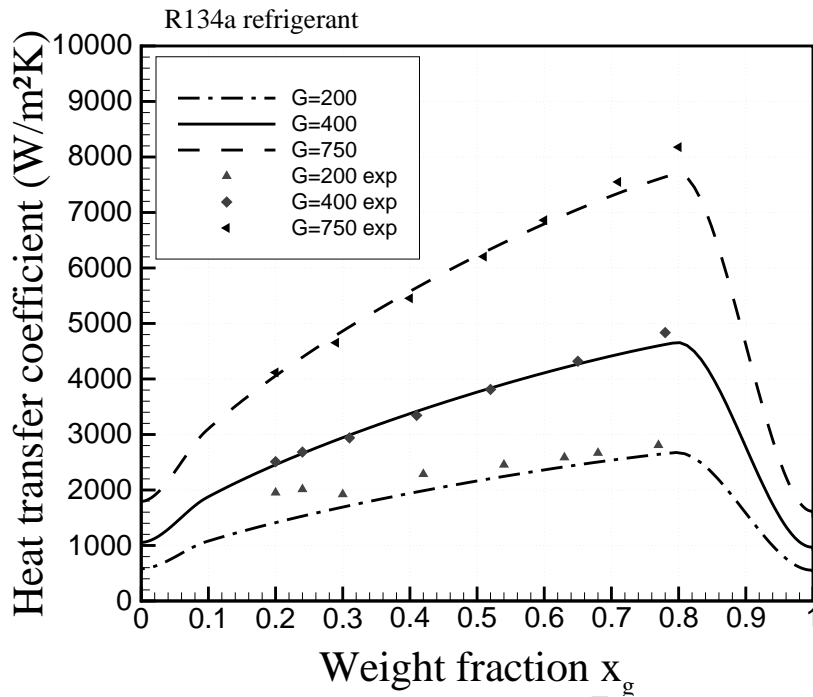


Fig. 6. Validation in condensation (R134a and R22 cases), using Shah's correlation [17]. Experimental data by Cavallini et al. [29]. Mass flux  $G$  in ( $kg/ms$ ).

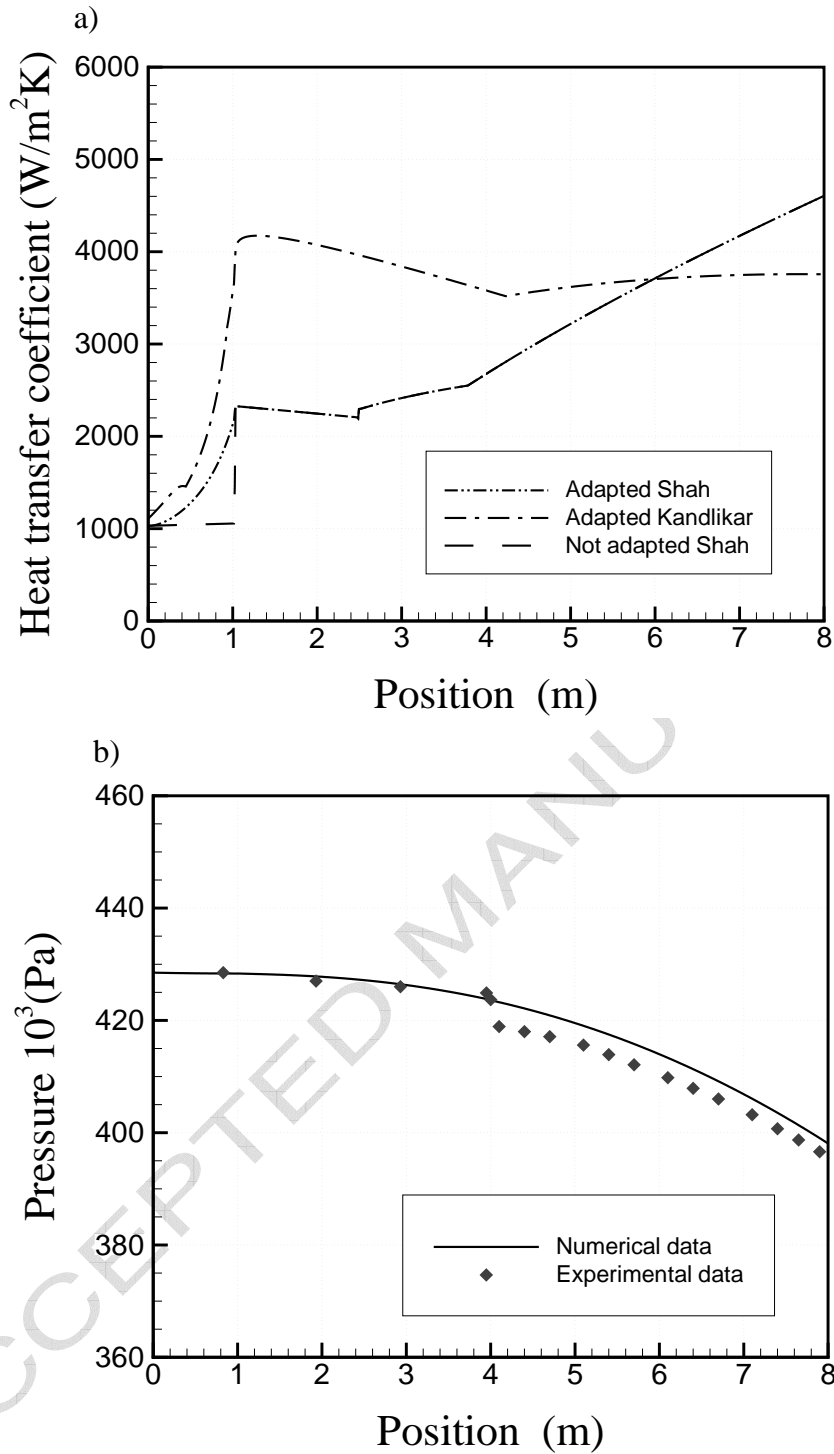


Fig. 7. Comparison between the numerical solution and experimental data from Jung and Didion [30]: a) heat transfer coefficient using adapted treatment correlation and not adapted with Shah's correlation [19] and Kandlikar's correlation [20]; b) pressure distribution.

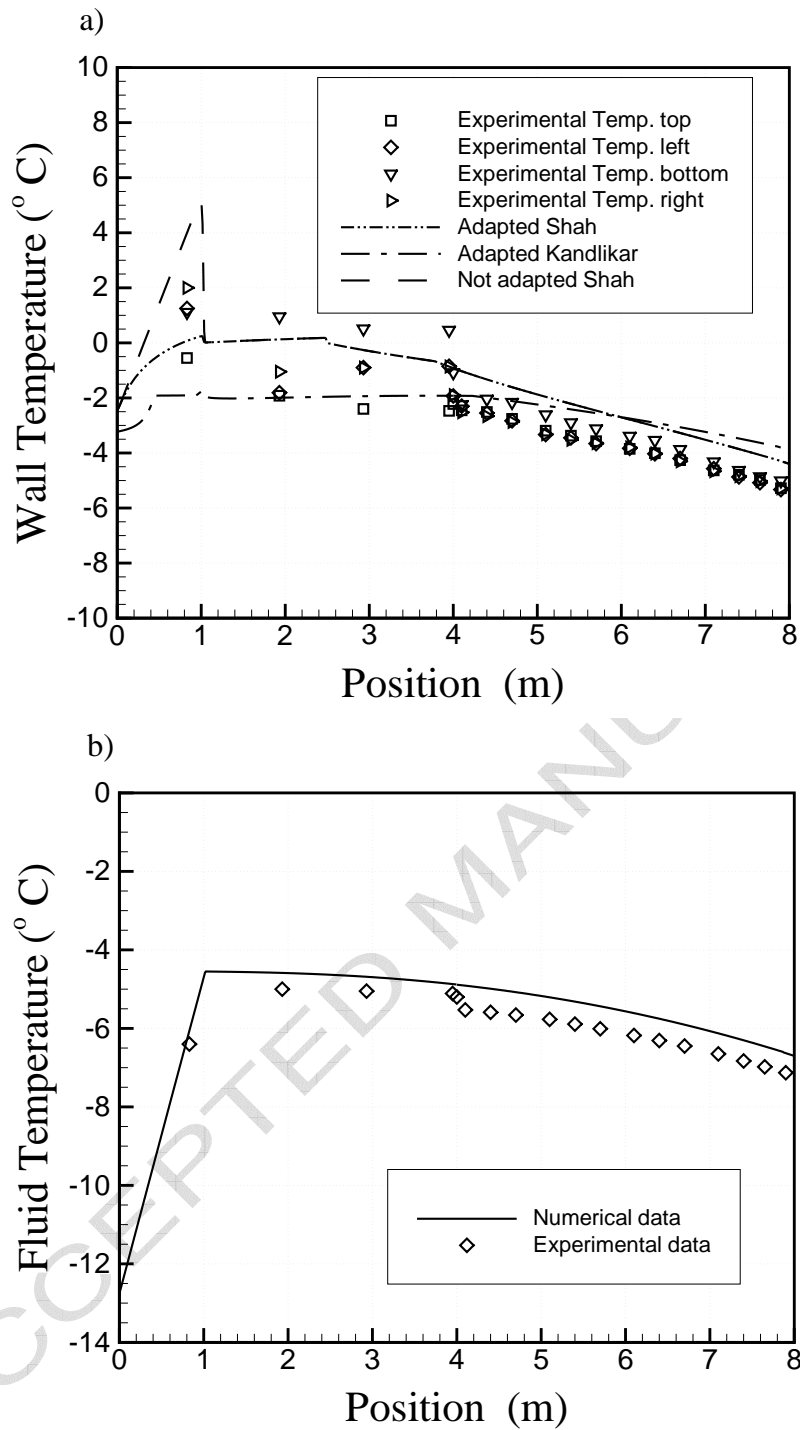


Fig. 8. Validation of numerical results using Shah's correlation [19] and Kandlikar's correlation [20]: a) the wall temperature, and b) the fluid temperature. Experimental data from Jung and Didion [30].

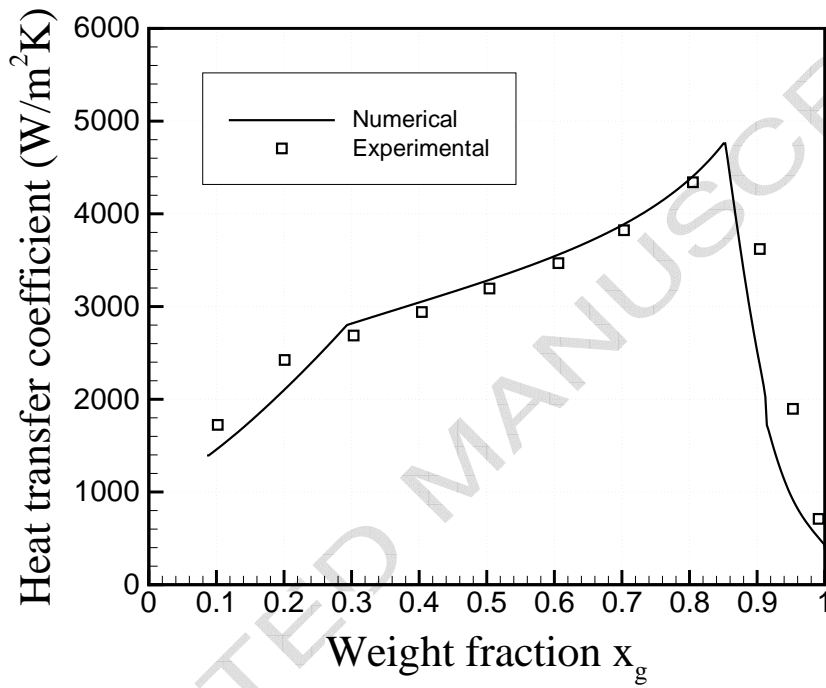


Fig. 9. Comparison of the heat transfer coefficient obtained in the numerical solution and experimental data in evaporation. Experimental data from Kattan et al.[21].

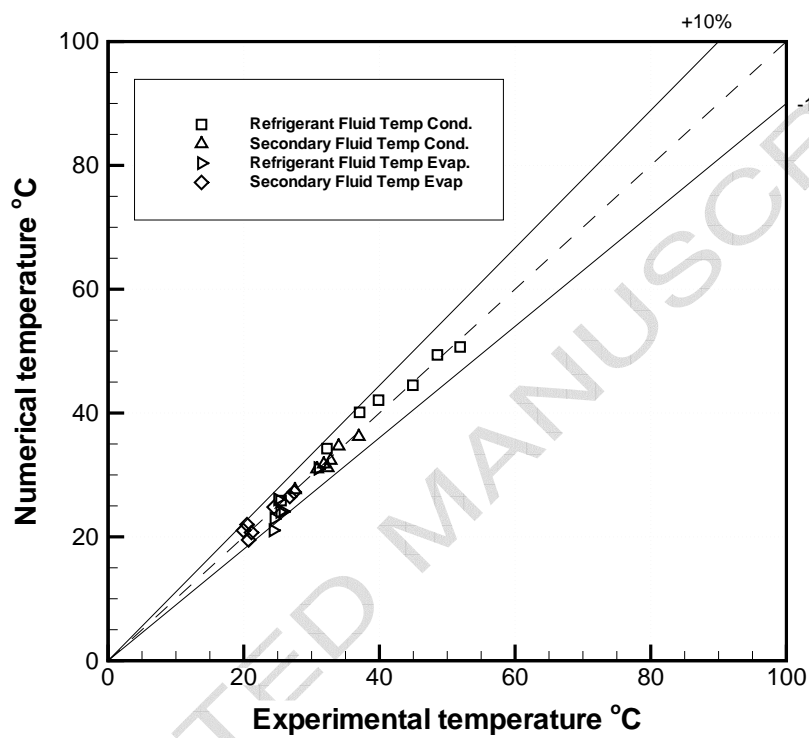


Fig. 10. Refrigerant and secondary fluid temperatures obtained in the numerical solution vs. experimental data in a double pipe heat exchanger.